The criteria in above-bandgap photo-irradiation in molecular beam epitaxy growth of heterostructure of dissimilar growth temperature

Kwangwook Park[1,2,3,4†], Jung-Wook Min[5,†], Gyeong Cheol Park[6], Sergei Lopatin[7], Boon S. Ooi[5], and Kirstin Alberi[1,*]

[1]National Renewable Energy Laboratory, Golden, Colorado 80401, USA

[2]Division of Advanced Materials Engineering, Jeonbuk National University, Jeonju 54896, Republic of Korea

[3]Hydrogen and Fuel Cell Research Center, Jeonbuk National University, Jeonju 54896, Republic of Korea

[4]Department of Energy Storage/Conversion Engineering of Graduate School, Jeonbuk National University, Jeonju 54896, Republic of Korea

[5]Photonics Laboratory, King Abdullah University of Science and Technology, Thuwal 23955, Saudi Arabia

[6]Electronics and Telecommunications Research Institute, Daejeon 34129, Republic of Korea

[7]Core Labs, King Abdullah University of Science and Technology, Thuwal 23955, Saudi Arabia

†Equally contributed to this work.
[*]E-mail: kirstin.alberi@nrel.gov

Abstract

Above-bandgap photo-irradiation is known to improve the low temperature growth of II-VI semiconductors, but the trade-offs in the substrate temperature and light source power density are not well known. We investigated these effects on the growth of ZnSe epilayers on GaAs. We find that the above-bandgap photo-irradiation can improve the ZnSe epilayer without substantially negatively impacting the underlying GaAs epilayer only if the laser power is below a threshold intensity. When the threshold is exceeded, the growth rate drops, the optical properties of ZnSe layer deteriorate and interface intermixing is enhanced. Together, cross-sectional transmission electron microscopy, energy dispersive spectroscopy and photoluminescence results suggest that photo-irradiation at moderate to high laser powers produces a trade-off in interface intermixing and planar defect formation. Most importantly, the damage produced by high laser powers does not start at the interface but instead in the bulk. Further flexibility for selecting the temperature and photo-irradiation intensities could be realized by turning on the laser irradiation after the ZnSe growth has been initiated, limiting the potential intermixing at the interface.

Pursuant to the DOE Public Access Plan, this document represents the authors' peer-reviewed, accepted manuscript. The published version of the article is available from the relevant publisher.

Introduction

In conventional epitaxial growth, careful control of the growth temperature through resistive heating at the back of the substrate is one of the most accessible and effective ways to deliver energy to impinging adatoms at the growth surface and promote the formation of highly crystalline epitaxial layers. When growing multiple layers and complex doping profiles, however, heating the entire epitaxial stack through the back of substrate can cause several issues. For example, thermally driven atomic inter-diffusion between neighboring layers and migration of dopant atoms can deteriorate device performance [1].

In-situ photo-irradiation of the substrate surface offers an additional route to deliver energy to the surface adatoms [2-4], allowing the substrate temperature to be lowered to prevent undesired modification to the underlying layers. We previously reported the effect of photo-irradiation on the low-temperature growth and interface formation of ZnSe on GaAs [5, 6] with a broadband 150 W Xe lamp. The goal of that work was to subtly influence the bonding arrangement at the hetero-interface. In this work, we investigate ZnSe epitaxy on GaAs with an intense, far-above-bandgap 248 nm KrF excimer laser, with the goal of substantially reducing the growth temperature of the entire ZnSe layer. The photon energy (5.0 eV) is well above the ZnSe bandgap (2.8 eV) as well as the dissociation energy of Se molecules (3.55 eV) [7]. We show that the high energy photo-irradiation enhances the optical and structural properties of the ZnSe epilayer, as expected from previous studies [8, 9]. The new insight that comes from this work is that there is a window of laser intensities and substrate temperatures that lead to beneficial improvement in the overall ZnSe and interface properties. Notably, the crystal quality of the ZnSe epilayer is improved when the combination of laser intensities and substrate temperatures is low, while deterioration is observed when the laser power reaches a threshold. We also identify the mechanism by which ZnSe growth breaks down under high laser powers. These results form the basis for selecting growth conditions to synthesize high quality ZnSe on GaAs without affecting the interface and also provide insight into ways in which photo-irradiation can improve the low temperature growth of other materials and heterostructures.

Pursuant to the DOE Public Access Plan, this document represents the authors' peer-reviewed, accepted manuscript.
The published version of the article is available from the relevant publisher.

Experiment

Heterostructures were grown on (100) GaAs substrates in an Omicron EVO25 molecular beam epitaxy (MBE) system with separate III-V and II-VI semiconductor growth chambers. The two chambers were equipped with conventional K-cells for the group-III and group-II elemental sources and valved cracker effusion cells for the group-V and group-VI elemental sources. The substrate temperature was measured with a k-Space BandiT band-edge thermometry system with an accuracy of ±1°C. Prior to growth, GaAs wafers were outgassed at 300°C in an ultra-high vacuum chamber. They were then transferred to the III-V growth chamber, where the native oxide was thermally desorbed at 610°C for 10 min under an As_2 overpressure. A 500 nm-thick homoepitaxial GaAs epilayer was grown first, followed by deposition of a thick amorphous As film by exposure to As_2 flux at room temperature for 1 h, which was used to protect the GaAs surface while the sample was transferred to the II-VI growth chamber. The formation of this protection layer was verified by observing the disappearance of the (2×4) GaAs surface reconstruction with reflection high-energy electron diffraction (RHEED). Once inside the II-VI chamber, the amorphous As film was thermally desorbed at 330°C in the absence of any group II or VI overpressures to produce a partially As-terminated surface. This was confirmed by the appearance of a (2×4) surface reconstruction having a faint 4× RHEED pattern [10]. Immediately after As film desorption, the substrate temperature was set to targeted values of 150°C, 200°C, 250°C and 300°C for ZnSe growth.

ZnSe growth was initiated by exposing the GaAs surface to Zn for 2 min with a beam equivalent flux (BEP) of 1×10^{-7} Torr to prevent the possible formation of secondary phases at the interface [11, 12]. The Se valve was then opened to begin the growth of a thick ZnSe layer. In the case of laser-assisted growth, photons were sourced from a 248 nm KrF excimer laser with a 25 ns pulse width, operated at a repetition rate of 10 Hz and focused into a square 7×7 mm spot size. The laser power at the illuminated area of the sample is controlled with a variable laser beam attenuator and was set to deliver laser powers of 3 mJ, 21 mJ, 63 mJ and 146 mJ (Table 1). The laser was turned on before the Zn exposure step and remained constant through the entire growth. Because the sample is rotated throughout growth, the laser irradiation resulted in a central circular region with some variation in the laser power at the very edges.

All ZnSe growths were carried out for 30 min under Se-rich condition [13, 14], resulting in pseudomorphic growth of epilayers below the critical layer thickness [15]. High-

Pursuant to the DOE Public Access Plan, this document represents the authors' peer-reviewed, accepted manuscript.
The published version of the article is available from the relevant publisher.

resolution X-ray diffraction (HRXRD), low-temperature photoluminescence (LT-PL), cross-sectional transmission electron microscopy (XTEM), and energy dispersive X-ray spectroscopy (EDS) measurements were performed with the sample pieces of the central region. A schematic of the growth procedure is displayed in Figure 1.

Result and discussion

We first investigate the effect of laser irradiation as a function of substrate temperature, ranging from 150 to 300°C. Figure 2(a) and 2(b) shows ω-2θ HRXRD patterns of samples grown without (Dark MBE) and with 3 mJ photo-irradiation (Laser MBE), respectively. In both figures, the peaks around -790 arcsec correspond to the ZnSe epilayer, while the peaks at 0 arcsec correspond to the underlying GaAs substrate and buffer layer. Figure 2(c) and 2(d) show the shift of the ZnSe epilayer peaks as a function of growth temperature in both sample groups. The peaks of the Dark MBE samples range from -720 arcsec at 150°C to -790 arcsec at 300°C. The peaks of the Laser MBE samples start at -760 arcsec in the sample grown at 150°C and quickly settle at around -790 arcsec in the temperature range of 200-300°C. The presence of distinct ZnSe-related peaks in all HRXRD patterns is due to the 0.27% lattice mismatch between ZnSe and GaAs [16]. In general, there are layer peak, substrate peak and Pendellösung fringes. The Pendellösung fringe is a result of constructive interference from X-rays reflected from the interface between the epilayer and substrate, and thus its spacing can be used to determine the epilayer thickness [EAG]. The ZnSe epilayer thicknesses were obtained from HRXRD curve simulations based on Equation 1 using the angular spacing inside Pendellösung fringes between the peaks of ZnSe and GaAs,

$$t\,[\text{Å}] = \frac{1.5406\,[\text{Å}]}{(\angle_{Peak1}\,[rad] - \angle_{Peak2}\,[rad]) \times cos\,\angle_{Substrate}\,\,[rad]} \qquad \text{(Eq. 1)}$$

where 1.5406 Å indicates the wavelength of Cu-Kα_1. $\angle_{\mathrm{Peak1}}$ and $\angle_{\mathrm{Peak1}}$ represent the peak positions of neighboring Pendellösung fringes, and $\angle_{\mathrm{Peak1}}$ - $\angle_{\mathrm{Peak2}}$ is the spacing between them. $\angle_{\mathrm{Peak1}}$ is the position of the peak associated with the substrate. The calculated thickness of the Dark MBE and Laser MBE ZnSe epilayers were approximately 140 nm, 115 nm, and 100 nm corresponding to the growth temperatures of ZnSe epilayers as 200°C, 250°C, and

Pursuant to the DOE Public Access Plan, this document represents the authors' peer-reviewed, accepted manuscript.
The published version of the article is available from the relevant publisher.

300°C, respectively for both the Dark or Laser MBE samples (Figure 2(e) and 2(f)). They are all within the critical layer thickness (~150 nm for this temperature range) [17] and exhibit negligibly small relaxation.

On the other hand, clear Pendellösung fringes are not present for ZnSe epilayers grown at 150°C. There are several possible reasons for the absence of Pendellösung fringes, such as the epilayer being too thin, a rough surface or interface, and poor crystallinity. In this case, we attribute their absence to poor crystalline quality in the bulk ZnSe layer due to insufficient adatom migration on the surface [18]. However, there is a slight distinction in the ZnSe peak position and linewidth between the Dark and Laser MBE samples (Figure S2). The peak corresponding to the ZnSe epilayer of the Laser MBE sample is shifted by only 30 arcsec relative to the samples grown at higher temperature, which is far less than the shift associated with the Dark MBE sample grown at 150°C (70 arcsec). The photo-irradiation conditions used here, however, do not appear to affect the ZnSe growth rate at temperatures higher than 200°C. Figures 2(e) and 2(f) show the thickness change of ZnSe epilayers of the Dark and Laser MBE samples as a function of growth temperature.

In earlier reports, above-bandgap photo-irradiation during MBE growth of ZnSe caused an increase in the growth rate due to enhanced dissociation of Se molecules at the growth surface [7]. Specifically, direct absorption of photons with energies greater than the dissociation energy of Se molecules (3.3 eV) have been reported to promote Se incorporation into the ZnSe film through photolysis. On the other hand, Fujita *et al.* found that the growth rate of ZnSe deposited by metal organic vapor phase epitaxy could be enhanced with low power densities (<200 mW/cm^2) of above-bandgap energy photons by a photo-catalytic effect [19]. Our results do not show any growth rate enhancement, even at comparable average power densities (see Table 1). We speculate that one possible reason for the difference may be the short pulse duration and relatively low repetition rate of our laser source, which could inhibit either mechanism from playing a significant role in the growth rate.

Further analysis of the impact of photo-irradiation on the radiative properties of the ZnSe epilayers was performed with LT-PL measurements. The PL spectra of the ZnSe epilayers were measured at 8 K with a 405 nm GaN laser operated at 1 mW, using a 435 nm long-pass filter to block the laser line. Two different gratings were used during the measurements; 150 l/mm to obtain wide spectral range PL and 600 l/mm to obtain detailed

Pursuant to the DOE Public Access Plan, this document represents the authors' peer-reviewed, accepted manuscript.
The published version of the article is available from the relevant publisher.

near-band-edge PL of ZnSe epilayers. The penetration depth of the 405 nm laser in ZnSe is around 100 nm, allowing us to probe the entirety of the grown ZnSe epilayer of the Dark and Laser MBE samples over a wide spectral range. The spectra of all samples other than the ones grown at 150°C consists of deep-level emission (DLE) below 2.4 eV and near-band edge emission (NBE) above 2.6 eV (Figure 3(a) and (b)). The PL spectra of the samples grown at 150°C (not shown) do not exhibit clear PL peaks, confirming the poor material quality as determined by the HRXRD measurements.

The DLE emission consists of self-activated (SA) and Cu-green emission associated with deeper defect complexes [16]. The NBE emission consists of donor-bound (DX) or free exciton emission (FX), Y_0 emission associated with recombination at dislocation states [10], deep-acceptor bound emission (I_1^{deep}) related to Zn vacancies, and donor-acceptor pair (DAP) emissions [20]. Since the excitonic emission is very sensitive to the crystal imperfections, the presence of excitonic emission serves as a proxy for lower non-radiative defect densities [21], and we therefore use the ratio of the NBE/DLE emission peak intensities as a simple indicator of crystalline quality. The NBE/DLE ratios are shown in Figure 3(e) for both sample sets. In the literature, the optimal ZnSe growth temperature is close to 300°C [22, 23]. Due to possible chamber dependent effects, the optimal temperature in our experiment falls closer to 250°C. The NBE/DLE ratio increases with increasing growth temperature up to 250°C in the Dark MBE sample set. On the contrary, the NBE/DLE ratio of the Laser MBE sample set is high in both the 200°C and 250°C samples through an increase in the NBE intensity. This is the clearest effect induced by photo-irradiation in this study and suggests that this method extends the growth temperature window in which it is possible to achieve a high NBE/DLE ratio. Comparatively, the NBE/DLE ratios of the Dark MBE samples vary across the 200-250°C range, requiring the grower to heat a very narrow temperature range.

Above 250°C, the NBE/DLE ratio in both sample sets falls due to an increase in the DLE emission intensity. However, some improvement is concurrently observed in the NBE emission. The ZnSe band edge emission includes several peaks associated with the strain-split heavy-hole (HH) and light-hole (LH) transitions [20, 21, 24]. Figures 3(c-d) and 3(f) show that the free excitonic emission corresponding to the light-hole transition (FX_{LH}) increases with the growth temperature in both the Dark and Laser MBE samples up to 300°C. The I_1^{deep} emission

Pursuant to the DOE Public Access Plan, this document represents the authors' peer-reviewed, accepted manuscript.
The published version of the article is available from the relevant publisher.

intensity associated with Zn vacancies (Figure 3(g) and 3(h)) also gradually decreases with increasing growth temperature in both sample sets.

The relative enhancement of the NBE/DLE ratio through an improvement of the NBE emission and reduction in DLE at 200°C suggest that photo-irradiation helps to suppress the formation of point defects that would otherwise form at such low growth temperatures. One possible mechanism for this improvement is enhancement of Se desorption mediated by photogenerated carriers, which can create a metal-rich surface with higher adatom mobilities that improve adatom incorporation [6]. The corresponding reduction in low energy and non-radiative recombination pathways can then lead to improved FX_{LH} emission. Matsumura *et al.* reported a similar conclusion [9]. However, we also find that the combination of the photo-irradiation and high growth temperatures leads to additional defects represented in the increased DLE evident in the Laser MBE sample growth at 300°C (Figure S3).

To investigate the effect of excessive above-bandgap photo-irradiation, the samples were grown by varying laser power from 0 mJ to 146 mJ while holding the growth temperature constant at 200°C. The laser power and photon flux densities are listed in Table 1. The HRXRD patterns of the samples corresponding to 0 mJ, 3 mJ, 21 mJ, and 63 mJ (Figure 4(a)) show a sharp ZnSe peak at around -790 arcsec and clear Pendellösung fringes, indicating that the ZnSe epilayer is of high crystallinity and the interface is abrupt. Figure 4(b) shows the thickness of the ZnSe epilayers obtained from HRXRD curve simulations. With increasing laser power, the ZnSe epilayer thickness increases slowly up to 150 nm. This result verifies that the ZnSe growth rate can be slightly enhanced through efficient cracking of Se molecules with sufficient photon flux. A point is reached, however, where the laser power damages the ZnSe. The sample grown under the highest laser power of 146 mJ showed a black circular mark with a radius of 1 cm (inset of Figure 4(b)), and the thickness could not be extracted from HRXRD curve simulation due to the absence of the Pendellösung fringes. The ZnSe peak position of this sample is also shifted to around -840 arcsec, which represents a strain higher than 0.27% (Figure 4(c)).

To better understand the origin of these changes, we have analyzed the samples with XTEM and LT-PL. Figure 5(a-h) shows TEM images obtained in a Titan Themis-Z TEM system. Figures 5(a) and 5(d) are images of two different areas of the Dark MBE sample grown at 200°C. Several planar defects, including stacking faults, were observed across the sample

Pursuant to the DOE Public Access Plan, this document represents the authors' peer-reviewed, accepted manuscript.
The published version of the article is available from the relevant publisher.

[25]. Figures 5(g) and 5(h) are high resolution images of *Defect 01* and *Defect 03*, shown in Figures 5(a) and 5(d), respectively. The density of these defects, identified by counting in representative TEM images, decreases in the sample grown under photo-irradiation. Figure 5(b) shows a large area XTEM image of the sample grown under 63 mJ of laser irradiation, while Figure 5(e) shows a high-resolution image of the *Defect 04*. Fast Fourier transform (FFT) images of selected areas in Figure 5(b) of ZnSe (*Area 1*), the ZnSe/GaAs interface (*Area 2*) and GaAs (*Area 3*) confirms the zincblende (ZB) structure in each layer and a highly coherent interface. Low temperature PL measurements, shown in Figures 6(a-d) and Figure S4(a), indicate that with increase of laser power to 63 mJ, the intensity of the ZnSe-based DLE and I_1^{deep} emission is suppressed and the spectral width of the DX_{LH} peak narrows slightly. This evolution denotes a corresponding reduction in point defects. Figure 6(b) shows the corresponding NBE/DLE ratios, which rise beyond 100 for ZnSe layers grown under photon energies of 63 mJ.

With further increase of laser power to 146 mJ, the planar defect density drops again in the ZnSe region near the GaAs interface, as shown in Figures 5(c) and 5(f). However, the layer thickness is confirmed to decrease to 15 nm (marked in Figure 4(b)). Notably, this sample does not exhibit any appreciable PL, likely due in part to its thinness. Despite the visible damage at the surface, the interface between the ZnSe and GaAs layers appears to be abrupt. Elemental EDS maps, presented in Figure 5(i) of the high-angle annular dark-field imaging area (Figure S1), corroborate the assessment that laser powers up to 146 mJ do not cause excessive intermixing on the order of atomic percent across the ZnSe/GaAs interface compared to the Dark (0 mJ) condition. PL measurements were additionally used as a more sensitive probe of laser-induced growth changes at the interface. PL emission from the GaAs epilayers beneath the ZnSe is shown in Figure 6(e) and Figure S4(b). Measurements were performed with a Nd:YVO laser (532 nm) to avoid absorption in the ZnSe epilayer. The excitation power was set to 0.31 mW, and a 150 l/mm grating and 570 nm long-pass filter were used. All samples, including the one grown under 146 mJ of photon energy, exhibited strong emission from the GaAs epilayer. The spectra consist of donor-bound (DX) and free (FX) excitonic emission, a carbon-bound emission (C_{As}) and its phonon replica (C_{As}'), and a parasitic emission (P) [5]. The parasitic emission has been observed in GaAs if the surface is exposed to excess Zn or Se [5, 6] and can thus serve as an indicator of intermixing at the scale of impurity levels

Pursuant to the DOE Public Access Plan, this document represents the authors' peer-reviewed, accepted manuscript.
The published version of the article is available from the relevant publisher.

across the ZnSe/GaAs interface. The intensity of the parasitic emission increases with increasing laser powers above 3 mJ and is especially pronounced in the sample grown under 146 mJ. The low energy tail has also been attributed to a complex mixture of elemental species in GaAs [11].

Together, the XTEM, EDS and PL results suggest that photo-irradiation at moderate to high laser powers produces a trade-off in interface intermixing and planar defect formation in bulk ZnSe. Most importantly, the damage produced by high laser powers (in this case, those near 146 mJ) does not start at the interface but instead in the bulk. A likely source of this damage is excessive desorption of adatoms (especially Se) over a prolonged growth period, resulting in a rougher surface and a presumably Zn-rich layer. Thus, a threshold laser power can be reached, even at low substrate temperatures, above which photo-irradiation is detrimental to ZnSe growth.

Conclusion

In this work, we investigated the effect of *in-situ* above-bandgap photo-irradiation on the growth of ZnSe epilayer on GaAs. We find that the above-bandgap photo-irradiation can improve the ZnSe epilayer without substantially negatively impacting the underlying GaAs epilayer only if the laser power is below a threshold intensity. When the threshold is exceeded, the growth rate drops and the optical properties of the ZnSe epilayer deteriorate. The deterioration is mainly initiated during bulk layer growth rather than at the interface, although some interfacial intermixing is observed. Photo-irradiation can aid epitaxial growth of dissimilar materials with different temperature sensitivities primarily by reducing the substrate temperature requirements, thereby allowing the topmost epilayer to be grown at nominally lower substrate temperatures without significant impact to the optical material quality. Further flexibility for selecting the temperature and photo-irradiation intensities could be realized by turning on the laser irradiation after the ZnSe growth has been initiated, limiting the potential intermixing at the interface.

Acknowledgement

Pursuant to the DOE Public Access Plan, this document represents the authors' peer-reviewed, accepted manuscript.
The published version of the article is available from the relevant publisher.

The authors acknowledge funding from the U.S. Department of Energy under contract DE-EE0006335, the Engineering Research Center Program of the National Science Foundation and the Office of Energy Efficiency and Renewable Energy of the Department of Energy under NSF Cooperative Agreement No. EEC-1041895. This work was authored in part by Alliance for Sustainable Energy, LLC, the Manager and Operator of the National Renewable Energy Laboratory for the U.S. Department of Energy (DOE) under Contract No. DE-AC36-08GO28308. Funding provided by the Office of Science, Basic Energy Sciences. The views expressed in the article do not necessarily represent the views of the DOE or the U.S. Government. The U.S. Government retains and the publisher, by accepting the article for publication, acknowledges that the U.S. Government retains a nonexclusive, paid-up, irrevocable, worldwide license to publish or reproduce the published form of this work, or allow others to do so, for U.S. Government purposes. The authors also would like to acknowledge support from National Research Foundation of Korea (NRF) grant funded by the Korea government (MSIT) (NRF-2020R1F1A1070471), and System Semiconductor Development Program funded by Gyeonggi-do.

Pursuant to the DOE Public Access Plan, this document represents the authors' peer-reviewed, accepted manuscript.
The published version of the article is available from the relevant publisher.

References

1. Z. Fan, K. Yaddanapudi, R. Bunk, S. Mahajan, and J. M. Woodall, J. Appl. Phys. **127** (2020) 245701 and references therein.
2. J. W. Cook Jr., D. B. Eason, R. P. Vaudo, and J. F. Schetzina, J. Vac. Sci. Technol. B **10** (1992) 901.
3. C. E. Sanders, D. A. Beaton, R. C. Reedy, and K. Alberi, Appl. Phys. Lett. **106** (2015) 182105.
4. N. C. Giles, K. A. Bowers, R. L. Harpers, S. Hwang, and J. F. Schetzina, J. Cryst. Growth **101** (1990) 67.
5. K. Park, J. Kim, and K. Alberi, J. Appl. Phys. **124** (2018) 225301.
6. K. Park, and K. Alberi, Sci. Rep. 7 (2017) 8516.
7. M. Ohishi, H. Saito, H. Okano, and K. Ohmori, J. Cryst. Growth **95** (1989) 538.
8. T. Fukada, N. Matsumura, Y. Fukushima, and J. Saraie, Jpn. J. Appl. Phys. **29** (1990) L1585.
9. N. Matsumura, T. Fukada, and J. Saraie, J. Cryst. Growth **101** (1990) 61.
10. K. Park, D. Beaton, K. X. Steirer, and K. Alberi, Appl. Surf. Sci. **405** (2017) 247.
11. S. Ahsan, and A. Kahn, Appl. Phys. Lett. **71** (1997) 2178.
12. G. Bratina, T. Ozzello, and A. Franciosi, J. Vac. Sci. Technol. B **14** (1996) 2967.
13. Q. Zhang, A. Shen, I. L. Kuskovsky, and M. C. Tamargo, J. Appl. Phys. **110** (2011) 034302.
14. S. K. Islam, M. C. Tamargo, R. Moug, and J. R. Lombardi, Phys. Chem. C **117** (2013) 23372.
15. B. J. Skromme, Annu. Rev. Mater. Sci. **25** (1995) 601.
16. C. Zhang, K. Alberi, C. Honsberg, and K. Park, Appl. Surf. Sci. **549** (2021) 149245.
17. J. Petruzzello, B. L. Greenberg, D. A. Cammack, and R. Dalby, J. Appl. Phys. **63** (1988) 2299.
18. M. Ohishi, H. Saito, M. Yoneta, and Y. Fujisaki, J. Cryst. Growth **117** (1992) 125.
19. S. Fujita, and S. Fujita, J. Cryst. Growth, **117** (1992) 67.
20. E. D. Bouttet, F. X. Zach, K. M. Yu, J. M. Walker, J. Cryst. Growth **147** (1995) 47.
21. II-VI Semiconductor Materials and Their Applications, Maria C. Tamargo, CRC Press (2001).

Pursuant to the DOE Public Access Plan, this document represents the authors' peer-reviewed, accepted manuscript.
The published version of the article is available from the relevant publisher.

22. D. Wlfframm, D. A. Evans, D. I. Westwood, and J. Riley, J. Cryst. Growth **216** (2000) 119.
23. Y. Qiu, A. Osinsky, A. A. El-Emawy, E. Littlefield, H. Temkin, and N. Faleev, J. Appl. Phys. **79** (1996) 1164.
24. C. d. Lee, S. I. Min, and S. K. Chang, J. Cryst. Growth **159** (1996) 108.
25. S. I. Molina, P. D. Brown, and C. J. Humphrey, J. Cryst. Growth, **156** (1995) 163.

Pursuant to the DOE Public Access Plan, this document represents the authors' peer-reviewed, accepted manuscript.
The published version of the article is available from the relevant publisher.

Figure captions

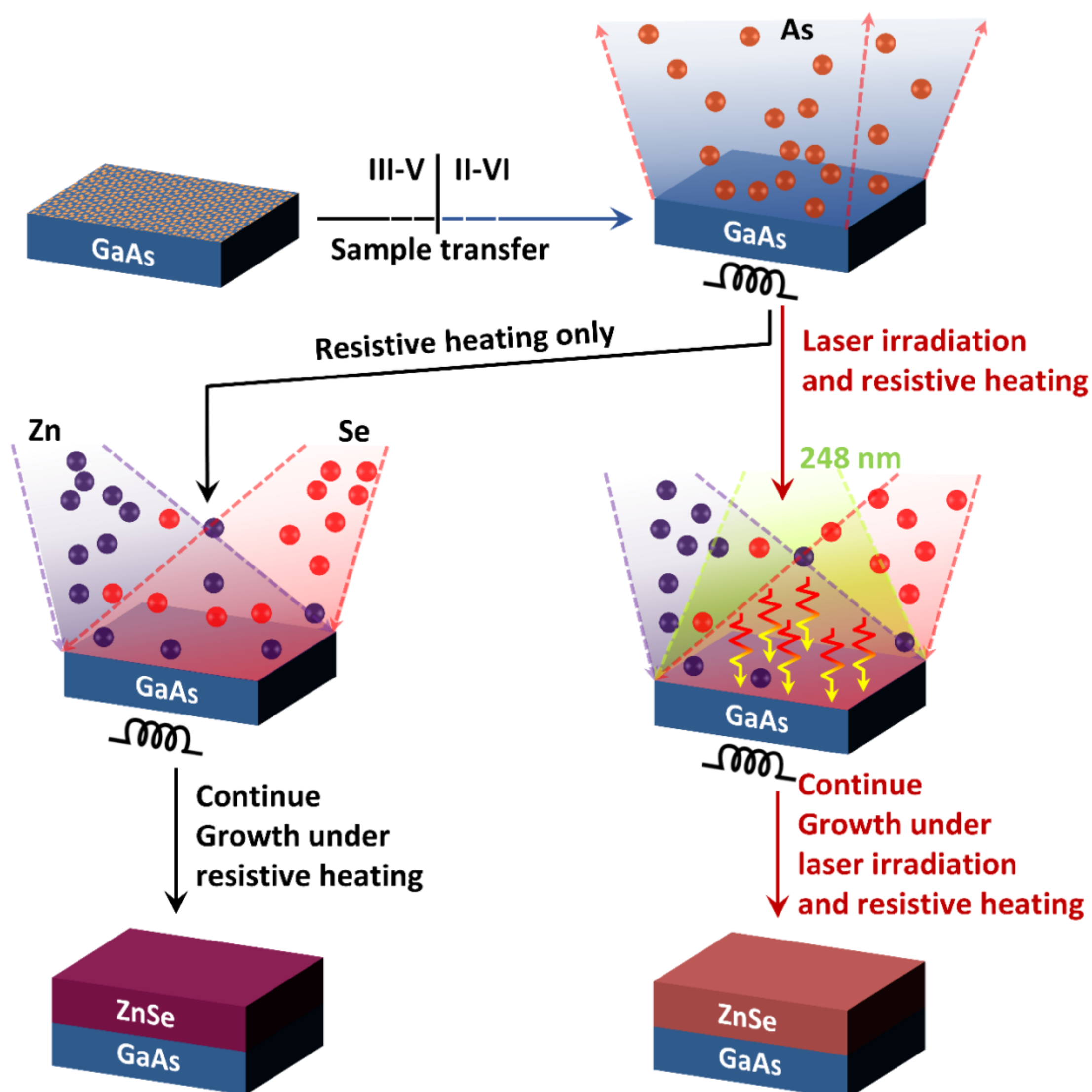

FIGURE 1. Schematic of the ZnSe growth on GaAs via resistive heating and photo-irradiation. A pulsed laser having 248 nm of wavelength was used to illuminate sample surface during growth.

Pursuant to the DOE Public Access Plan, this document represents the authors' peer-reviewed, accepted manuscript.
The published version of the article is available from the relevant publisher.

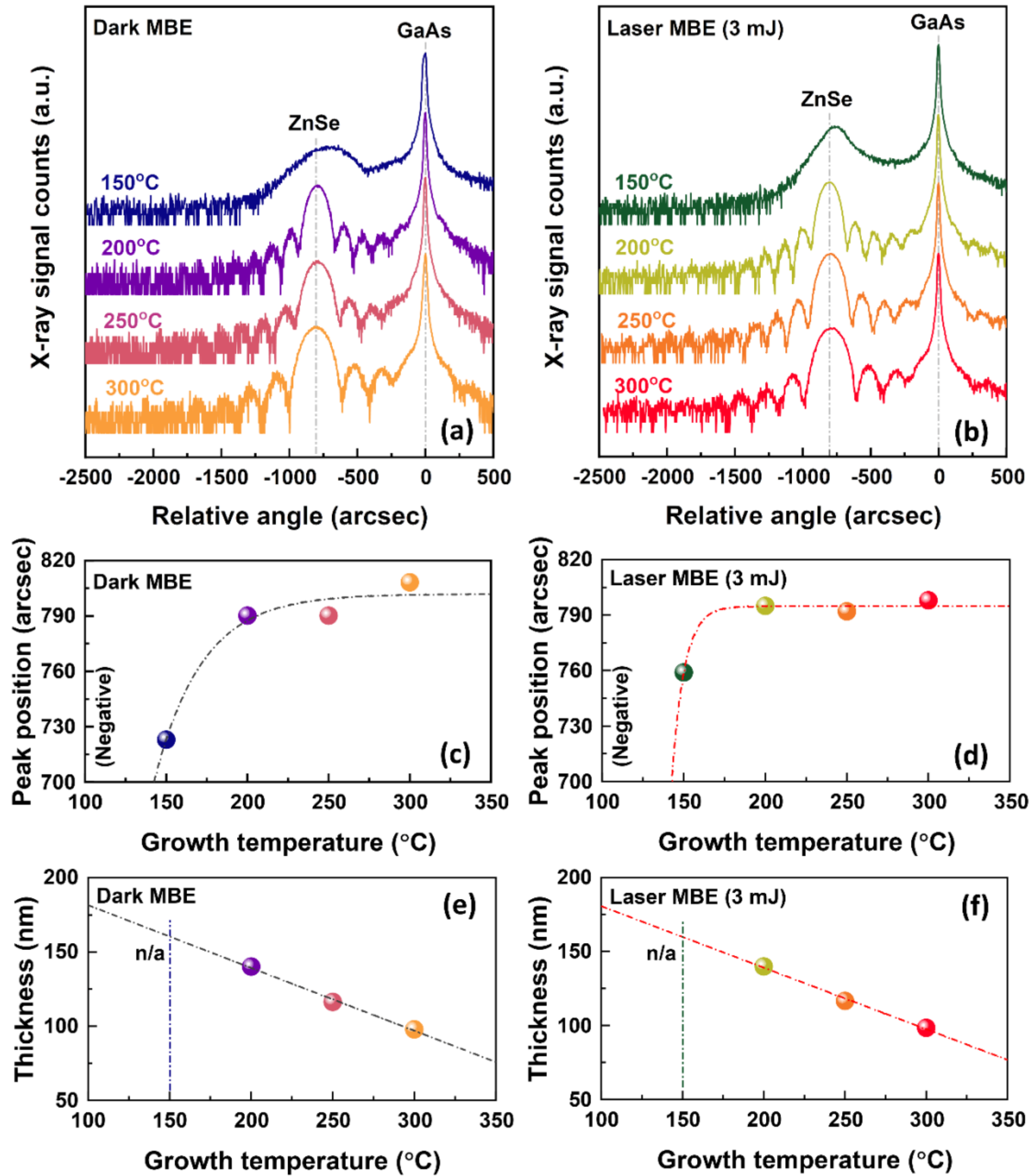

FIGURE 2. (a) and (b) shows HRXRD curves of the samples corresponding to dark (resistive heating) MBE growth and laser MBE growth, respectively. Based on (a) and (b), the changes in peak position and thickness of ZnSe layer were obtained. (c) and (d) presents the shift of peak position corresponding to ZnSe layer with the change of growth temperature. (e) and (f) shows the changes in thickness of ZnSe layer as a function of growth temperature, respectively.

Pursuant to the DOE Public Access Plan, this document represents the authors' peer-reviewed, accepted manuscript.
The published version of the article is available from the relevant publisher.

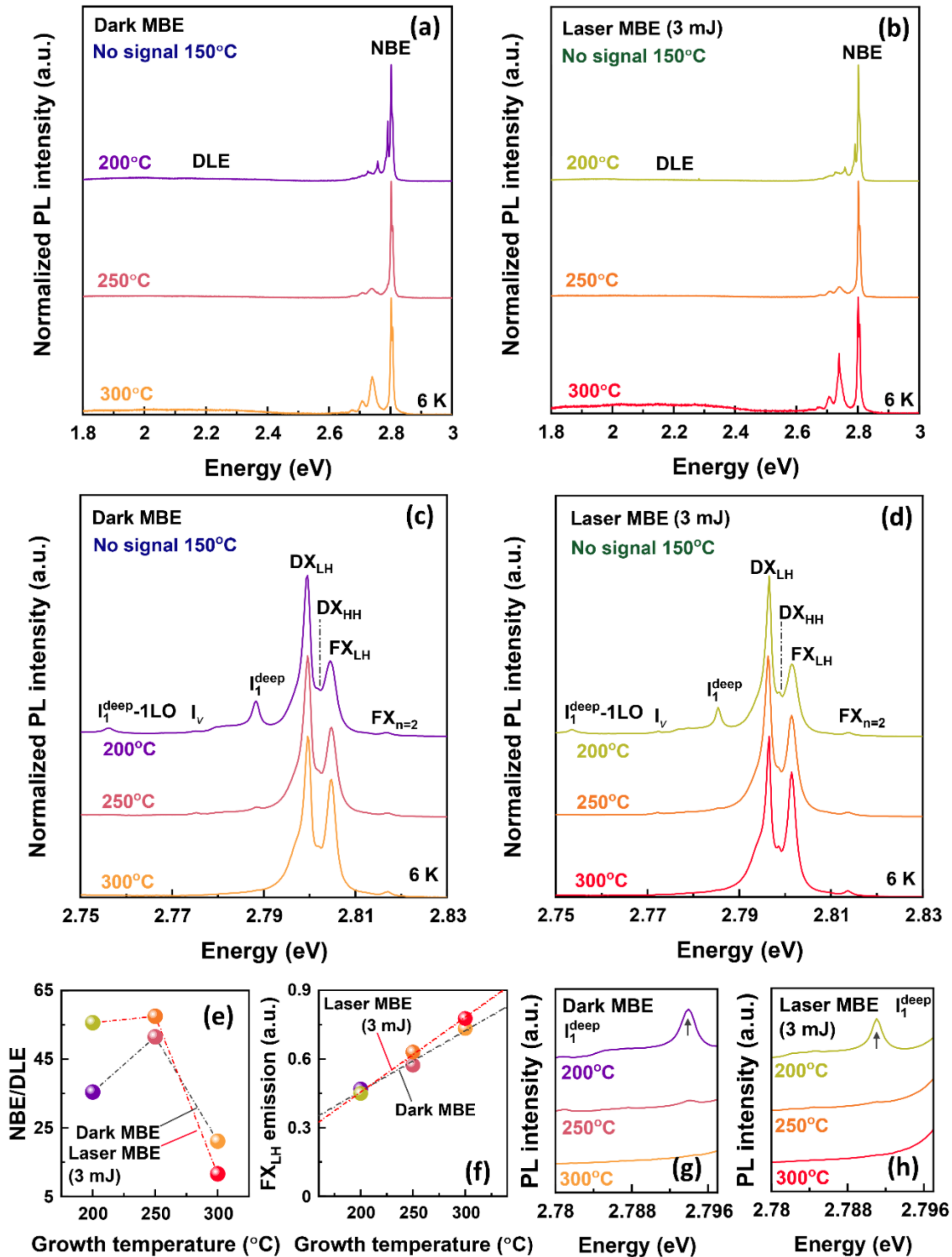

FIGURE 3. (a) and (b) represents LT-PL (6 K) spectra in the range of 1.8-3.0 eV of the samples corresponding to dark and laser MBE growth, respectively. (c) and (d) shows LT-PL (6 K)

Pursuant to the DOE Public Access Plan, this document represents the authors' peer-reviewed, accepted manuscript.
The published version of the article is available from the relevant publisher.

spectra of the samples of (a) and (b) within NBE range, respectively. (e) represents the NBE/DLE ratio of the two sample groups. (f) shows the enhancement of the FX_{LH} emission with increase of growth temperature. (g) and (h) represents the suppression of I_1^{deep} emission with increase of growth temperature of Dark and Laser MBE samples, respectively.

Pursuant to the DOE Public Access Plan, this document represents the authors' peer-reviewed, accepted manuscript.
The published version of the article is available from the relevant publisher.

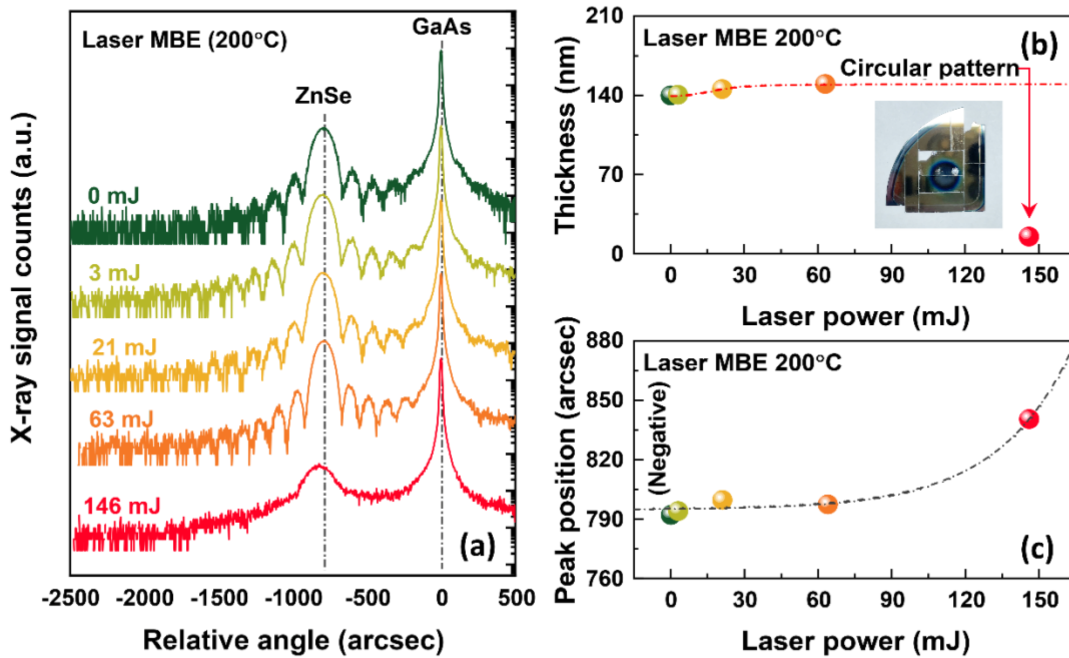

FIGURE 4. (a) represents HRXRD curves of the laser MBE sample grown at 200°C. (b) and (c) are thickness change and peak position shift as the functions of the energy of pulsed laser, respectively. The inset in Figure 4(b) shows photographic image of the sample corresponding to the laser power of 146 mJ.

Pursuant to the DOE Public Access Plan, this document represents the authors' peer-reviewed, accepted manuscript.
The published version of the article is available from the relevant publisher.

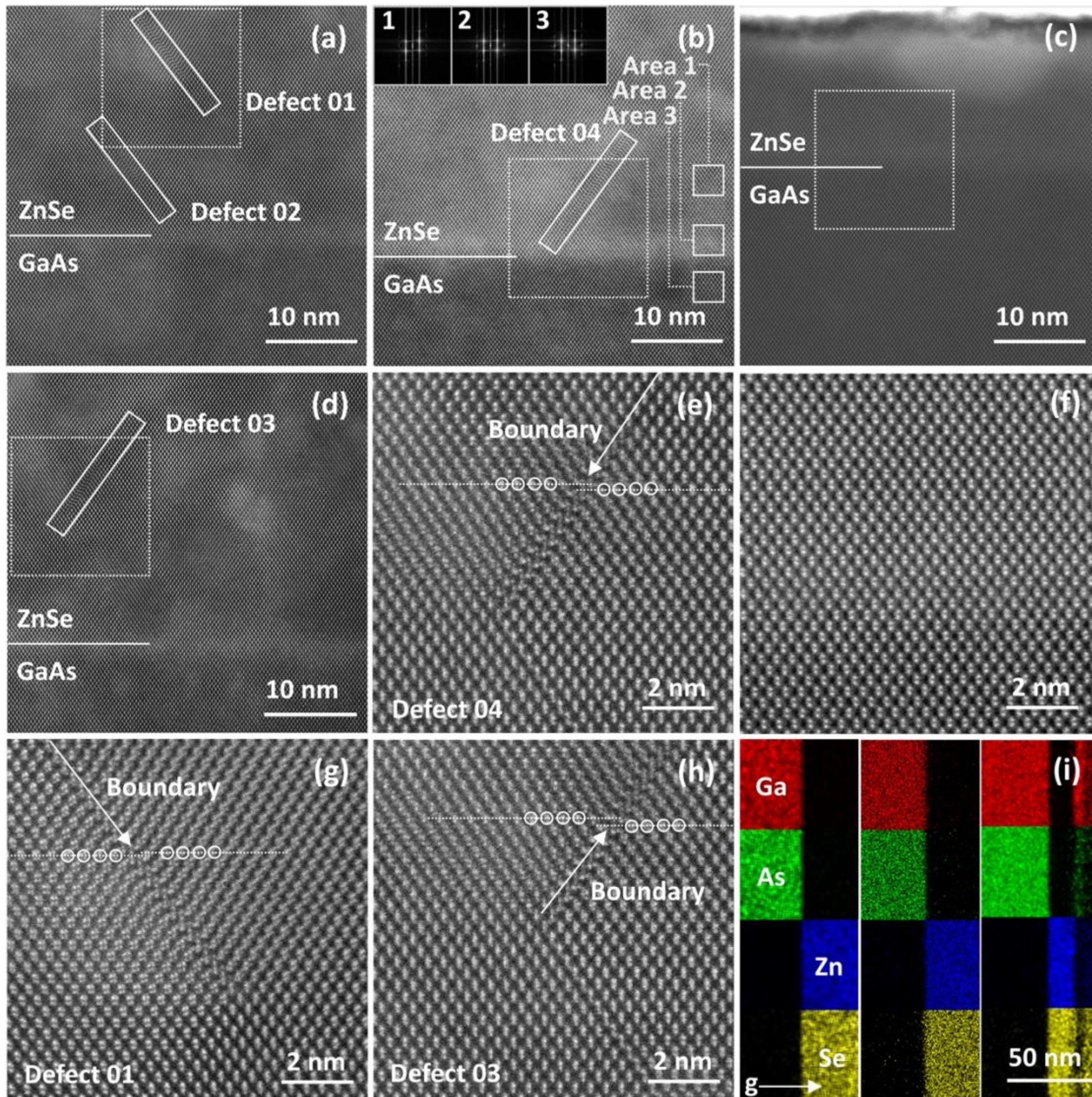

FIGURE 5. (a) and (d) are TEM images of sample corresponding to 0 mJ. (g) and (h) are HRTEM images of selected areas of Figure 5(a) and 5(d). (b) and (c) are TEM images of samples corresponding to 63 mJ and 146 mJ, respectively. (e) and (f) are their corresponding HRTEM images of selected areas. (i) shows EDS maps of samples corresponding to 0 mJ, 63 mJ and 146 mJ, respectively (from left to right). Inset in Figure 5(b) represents FFT images of the areas (1), (2) and (3) where *g* indicates the growth direction.

Pursuant to the DOE Public Access Plan, this document represents the authors' peer-reviewed, accepted manuscript.
The published version of the article is available from the relevant publisher.

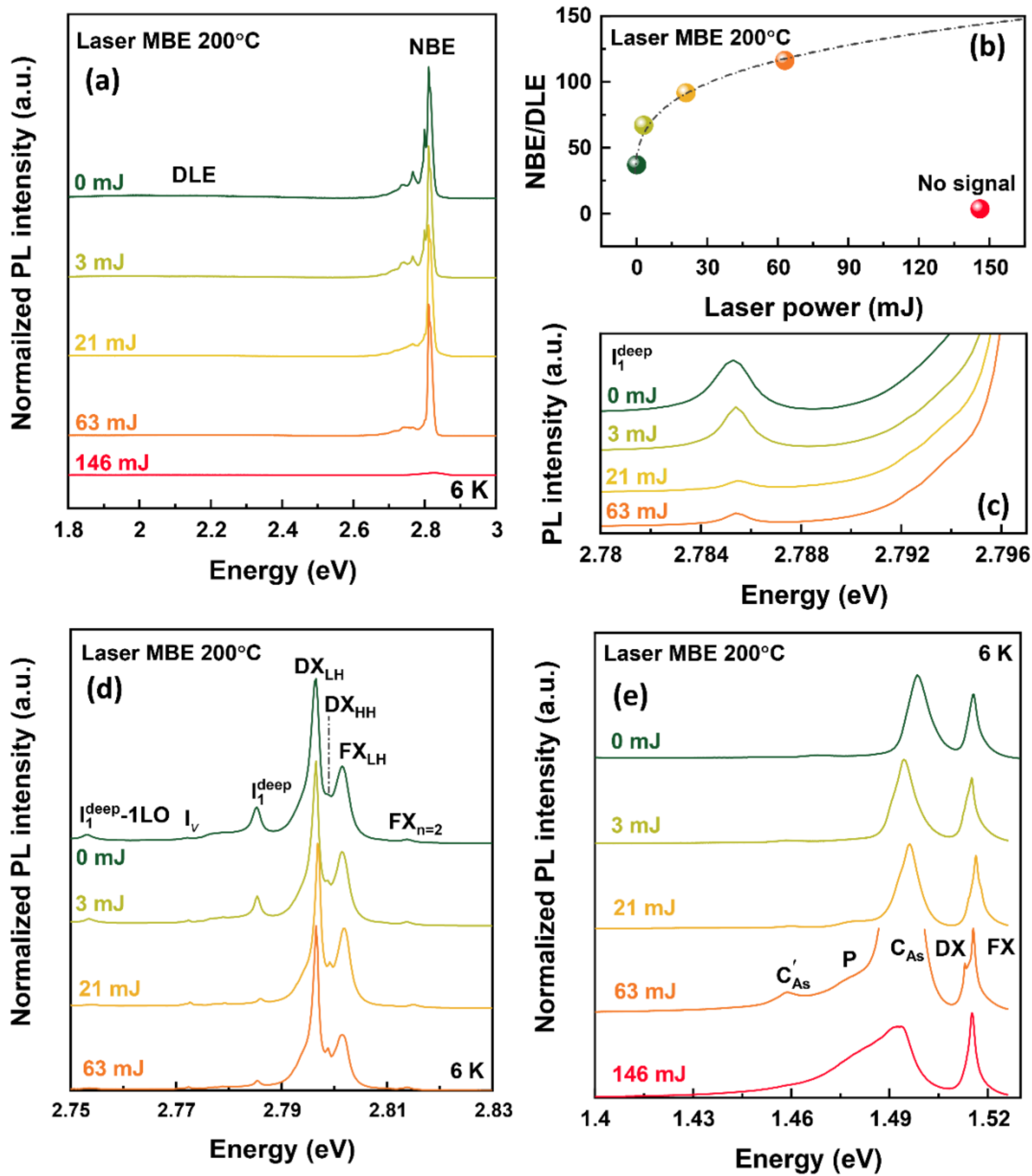

FIGURE 6. (a) shows LT-PL (6 K) PL spectra of laser MBE samples in a wide. (b) presents NBE/DLE ratio change as a function of energy of pulsed laser which obtained from Figure 4(a). (c) shows spectral width of the NBE emission. (d) and (e) represents LT-PL (6 K) PL spectra of the samples which probed by 405 nm and 532 nm lasers to see emission from ZnSe and GaAs layers of the samples, respectively.

Pursuant to the DOE Public Access Plan, this document represents the authors' peer-reviewed, accepted manuscript.
The published version of the article is available from the relevant publisher.

Table 1. Power density and photon flux density of 248 nm KrF excimer laser used in the sample growth. The repetition rate and spot size were 10 Hz and 7×7 mm^2, and the laser power at the illuminated area of the sample is controlled with a variable laser beam attenuator.

Laser power (mJ)	Average Power density (mW/cm^2)	Photon flux density ($\times 10^{16}$ photons/$cm^2 \cdot s$)
3	60	7.5
21	430	53.8
63	1,290	161.2
146	2,980	372.5

Pursuant to the DOE Public Access Plan, this document represents the authors' peer-reviewed, accepted manuscript.
The published version of the article is available from the relevant publisher.